OTKA (NKFIH) K 112114 Grant – Final report

Combined micro-nanotechnology supported by local probe analytical techniques: from pattern formation toward applications

Principal Investigator:	Zsolt Zolnai
Hosting Institution:	Institute of Technical Physics and Materials Science, Centre for Energy Research (MFA EK), Hungarian Academy of Sciences (HAS)
Project duration:	2014. 09.01.-2018.08.31.

Summary of the research activities performed between 2014 - 2018

We note that within the reorganization of the academic institutional network, MFA has joined the Centre for Natural Sciences of the HAS in 2012, but later has been relocated and from 2015 MFA joined the Centre for Energy Research of the HAS. In the period 2014-2015 several projects including this one were recontracted and due to the delay – despite that this proposal has officially started in 2014 – the first annual report has been submitted to NKFIH in 2016.

Participants of the project:

-Zsolt Zolnai (PI), senior participant
-Gábor Battistig, senior participant
-Attila Lajos Tóth, senior participant
-András Deák, participant
-Norbert Nagy, participant
-Dániel Zámbó, participant, PhD student
-Eszter Gergely-Fülöp, participant (until 2015.03.31.), PhD student
-Szilárd Pothorszky, participant (from 2015.04.01.), PhD student

The list of project participants is in accordance with the list of members given in the project proposal submitted in 2014. Only one modification has been initiated, Eszter Gergely-Fülöp completed her PhD work in 2015 and left the institute. Instead, Szilárd Pothorszky PhD student joined the project from the spring of 2015 until 2018. We applied for the substitution that has been permitted by the NKFIH Office.

Outcomes of the project

-The laboratory platform at MTA EK MFA for preparation of samples comprising colloidal nanoparticulate monolayers on different substrate surfaces has been developed further. Also, the measurement infrastructure for single particle optical scattering spectroscopy has been introduced and significantly improved.

-The project provided knowledge transfer in the field of preparation and nanoscele manipulation of plasmonic nanoparticulate systems. We widened our activity in the optical and structural

characterization of single nanoparticles and their ensembles. We aimed to study the effect of the controlled local environment on the optical properties of the nanoparticles. Also, research was targeted to find the role of precise placement of the particles with respect to their spatially varying surroundings in the modification of the near-field effects and far-field optical scattering behaviour. Such research is indispensable for the development of nanosensors and nanoscale manipulation techniques.

-The project resulted in 32 publication: 20 journal papers and 12 conference presentations. The cumulative impact factor for the papers is 71.6.

-Research activities related to the project helped the three participating PhD students in getting experience for their professional work. All of the students: Eszter Gergely-Fülöp, Dániel Zámbó, and Szilárd Pothorszky defended their PhD thesis during the project period.

In the following we summarize the main objectives and results of the project.

Ion beam-induced modification of silica nanoparticles

According to the work plan, in a first step, the 40 keV Ar^+ ion irradiation-induced reorganization of Langmuir–Blodgett (LB) monolayers of colloidal silica nanoparticles (NPs) deposited on silicon substrate was investigated in a wide range of ion fluences. The cluster formation, average cluster size, the role of ion beam-induced charging and discharging, heating effects, the ion beam-induced viscous flow and the swelling of the underlying Si substrate have been analyzed. We found that at low ion fluences particle charging and Coulomb repulsion forces govern the reorganization process, while at high ion fluences ion beam-induced viscous flow and hydrodynamic forces between the particles and the underlying substrate play major role. Two different types of patterns: small compact clusters of few particles and long chain-like clusters of dozens of particles were observed by SEM analysis. The dynamics of the reorganization process was treated analogous to the Tanaka–Araki model, with or without considering hydrodynamic interaction between the particles. This work was accomplished in cooperation with the Rudjer Boskovic Institute, Zagreb, and the results were published in [1]. These experiments help to understand the different processes taking place when ion beam lithography patterning is applied through colloidal nanoparticulate masks.

Local probe analytical techniques for the characterization of nanoparticulate systems

The above experiments focused on NPs in the 200-500 nm size range. In this case, different analytical tools: field emission scanning electron microscopy (FESEM), atomic force microscopy (AFM), and Rutherfod backscattering spectrometry (RBS) are powerful characterization techniques at the nanoscale. Such techniques are accessible long at and nearby our institute. However, especially in plasmonic applications the NP size is typically in the 10-100 nm range. In this case, the introduction of further powerful techniques with spatial resolution in the nm-range are essential to study the geometry, composition, and optical properties (especially the surface plasmon resonance, SPR) of individual NPs and find correlation between these features.

Following our research plan, a measurement platform aiming single-particle optical scattering spectroscopy was developed with the partial support of this project. Optical elements and a ceramic sample holder with a XYZ piezo controller were installed to the optical microscope (Olympus BX51) combined with an aberration corrected imaging spectrometer (IsoPlane SCT 320 equipped with a

PIXIS 400BRX cooled CCD camera, Princeton Instruments). Thus single particle optical scattering measurements become available.

From 2015, through collaboration with the International Institute of Accelerator Applications (IIAA), University of Huddersfield, UK, we performed medium energy ion scattering (MEIS) experiments with 100 keV He^+ ions. MEIS allows quantitative 3D analysis of the shape, size, and atomic composition of NPs of 10-100 nm size, with depth resolution of about 0.5 nm at the surface. The MEIS spectra were compared to RBS-MAST [L1] simulations performed on artificial 3D model cells. The reliability of our RBS-MAST simulation code in the analysis of nano-patterned surfaces has been proven via an intercomparison with other 2D and 3D codes: CORTEO, STRUCTNRA, and F95-Rough. This work was cooperation with the Max Planck Institute in Garching, the Nuclear Physics Institute of the Czech Academy of Sciences and with the RQMP in Montreal, Canada. The results were published in [2].

Note, for the correct interpretation of MEIS spectra it was necessary to take into account dual scattering events for the analysing He+ ions besides single scattering events. So far this problem has not been widely discussed in the literature for the energy range applied in MEIS. We performed Monte-Carlo simulations and, also, introduced an analytical model to estimate the effect of dual scattering in the MEIS spectra. Measured and calculated DS spectra show good agreement for thin Au layers and Au nanospheres. The results were presented as a talk at the IBA23 Conference in Shanghai, China, in 2017 [3], and as a poster at the HRDP9 conference in Uppsala, Sweden, in 2018 [4].

Ion beam-induced modification of gold-silica core-shell nanoparticles

From the second year of the project the ion irradiation-induced modification of Au-silica core-shell (CS) nanospheres (NS) and nanorods (NR) was studied with MEIS, single particle optical scattering spectroscopy, and FESEM analysis.

The core/shell diameter was 25 nm/40 nm for the NSs and the core/shell diameter×length was 14 nm×46 nm/40 nm×66 nm for the NRs. The nanoparticles (NPs) were deposited on Si substrate by LB technique, and then exposed to ion bombardment as a nanofabrication tool. In general, ion-solid interactions on the nanoscale are of special interest, and so far the radiation resistance of the SPR properties of metal NPs has been scarcely studied. In this project ion irradiation was performed under largely different conditions, by 30 keV Ar^+, and 2.8 MeV N^+ ions to cover a wide range of ion-nanoparticle interactions. Ion beam-induced mixing, sputtering, clustering, charging and heating may induce geometrical and structural changes of individual NPs and their clusters. Accordingly, the SPR excitation of Au-silica NPs can be modified as the excitation strongly depends on the shape (aspect ratio) of NPs, inter-particle distance, the thickness of the particle shell and the dielectric properties of the substrate. Especially, the longitudinal SPR (LSPR) of gold nanorods can be strongly affected by the particle shape and the environment.

From MEIS and FESEM the thickness of the silica shell and the diameter of the Au cores were determined. As a result, low energy Ar^+ irradiation causes the removal of the forepart of the silica shell through sputtering. The Au core is still present but it gets closer to the surface of the nanoparticle within 1 nm. Interestingly we found quite similar effect for high energy N^+ and low energy Ar^+ bombardment, despite the big difference in the irradiation parameters (sputtering yield, nuclear and electronic energy loss). For spheres at the highest ion fluences we observed the decrease of the transverse particle diameter by about 8 nm and 9 nm for N+ and Ar+, respectively, mainly due to the reduction of the silica shell. For nanorods the transverse diameter is reduced by 5 and 11 nm for N+ and Ar+, respectively.

Optical reflection measurements under normal incidence conditions and dark field single particle microspectroscopy measurements with large angle of incidence were performed on the irradiated and unirradiated samples in the visible range to correlate the geometry changes with the Au optical excitation spectra. For NSs slight blueshift of the SPR peak maximum and reduction of the scattered intensity at higher wavelengths (around 700 nm) has been observed for most of the irradiated samples. This effect can be due to the reduction of the silica shell on top of the Au NPs that is accompanied by the decrease of the refractive index of the environment.
For the NRs the LSPR peak shows significant blueshift for the Ar+ irradiated samples because the length of the Au rods decreases. On the other hand, no such effect can be observed for N+ irradiation. In summary, the geometrical changes can be well correlated with the optical properties. In addition, the NPs show considerable radiation resistance against the bombardment of energetic ions.

The above described results were presented on posters at the High Resolution Depth Profiling conference (HRDP8) in London, Canada, in 2016 [5], and at the IBA23 Conference in Shanghai, China, in 2017 [6, 7].

As charging was found to take place in ion irradiation-induced rearrangement of NPs we performed experiments to monitor surface potential buildup and the behaviour of the NPs in the presence of high electric fields. The RBS technique combined with a tunable electron source was appropriate to generate, control, and characterize strong surface potentials on insulating glass targets covered with Au NPs.
On a uniquely produced silica target glass doped with Er, Te, and Zn in the subsurface region [8, 9] we showed that the presence of the positive surface potential splits the RBS spectra for the He^+ and He^{2+} charge states. From the split the surface potential can be determined, independently for each target atomic component. We used the same concept for Au NPs deposited on glass and in presence of high electric fields found reduction and strong distortion of Au NPs uncovered with silica shell. However, no such changes were observed for Au-silica core-shell NPs thus showing the protective nature of the dielectric shell. The results were presented at the Advanced Nanomaterials conference (ANM2016) in Aveiro, Portugal, in 2016 [10].

We performed He^+ RBS/channeling angular scans on (100)Si substrates covered with Au NPs to monitor the low angle scattering (dechanneling) effect of the NPs during sample charging. Using the electron flood gun, substrate Si charging was or was not allowed during the angular scans. We found that Au NPs cannot hold higher potential than 1-10 V, even for high Si surface potential buildup of several kilovolts.

The results were presented on a poster at the 22nd International Conference on Ion Beam Analysis (IBA22), Opatija, Croatia, in 2015 [11].

Optical scattering spectroscopy on individual nanoparticles, assembled nanoparticles, and asymmetric nanoparticles

As single particle optical scattering measurements become available, efforts have been made aiming to relate the visible light excitation spectra of different Au nanoparticle clusters to their 2D or 3D structure. Changes of the interparticle distance can have a significant impact on the frequency of the coupled modes in the plasmon excitation spectra. A number of different configurations were checked, e.g., optical simulations were carried out by boundary element method (BEM) for linear chains of Au NPs, and for 2D and 3D hexagonal close packed structures with varying interparticle distances [12]. Region-selectively surface modified gold nanorods assembled with spherical gold particles of different sizes [13, 14], and compact clusters prepared from PEG-coated and amino-PEG

covered gold NPs were also studied [15, 16]. Also, the preparation and characterization of 2D metallic NP and void films derived from a colloidal template layer has been performed [17].

We reported the formation of single chain Au NP rings, as a special configuration of individual NPs. The parallel nanoparticle assembly was carried out by means of capillary lithographic experiments over a silicon substrate supported polystyrene microparticle Langmuir−Blodgett monolayer, using high purity aqueous solution of PEGylated gold NPs. [18]. During dewetting on the high purity surface of Si unwanted deposition of the gold NPs is minimized and precise placement of the gold NPs can be achieved. The use of gold nanoparticles as tracer objects can be generally utilized in experiments where wetting−dewetting properties should be investigated on structures with small dimensions. On the other hand, these structures might show advantageous properties compared to single particles or other ringlike structures reported earlier, due to strong coupling between the individual particles, allowing them to be used as a potential SERS substrate.

The above works confirm that by using optical spectroscopy, the cluster formation related spectral changes due to plasmon couplings can be monitored in solution or on solid substrate surfaces. Consequently, interparticle distances can be estimated from the spectral response.

When individual plasmonic NPs are placed in an environment that is inhomogeneous on the nanoscale, like in the case of nanopatterned substrate surfaces, then changes in the SPR are expected, due to the modified boundary conditions. Therefore, the effect of inhomogeneous environment around individual Au nanoparticles on their optical scattering properties has been studied. An interfacial templating preparation method was shown that enables the fabrication of “mushroom” shaped NPs, where a gold particle is only partially covered by the silica cap. From the measured and simulated single particle spectra it was shown that the redshift of the SPR peak is influenced by the extent of coverage of the gold core by the silica cap. This effect is similar but reverse of the ion irradiation-induced effect where the silica cap was removed from the top of Au NPs and slight blueshift of the SPR peak was observed. The results on mushroom shaped NPs were published in [19].

In another work it was shown that scanning-probe (AFM) and optical measurements performed on individual Au NPs provide direct experimental evidence on the inhomogeneous ligand distribution of tip-selectively cysteamine-modified gold nanorods. At higher cysteamine concentration, a well-defined patch is formed at the tips of the NRs. In accordance with this, the blue shift of the LSPR can be observed due to the lower effective dielectric value in the near-field at the rod tip. The results show that the modification of the local environment around the rod tip can be well detected via the LSPR signal. The results were presented in [20-23].

Deposition and optical characterization of individual nanoparticles on nanopatterned surfaces

After the single-particle optical scattering spectroscopy platform was developed and experience and state of the art knowledge on the effect of shape, composition, and local environment changes on the SPR of individual gold NPs and their assembles has been gathered, in the third year, according to the work plan, the optical scattering (SPR) properties of nanorods deposited on nanopatterned surfaces has been studied. As a widely used transparent conductive material to support plasmonic nanoparticles, indium tin oxide (ITO) was chosen. Gold nanorods (GNR) with average aspect ratio of 2.5 were used as good candidates for plasmonic sensors due to their narrow LSPR peak and relatively low damping (accompanied with low FWHM). In this case the LSPR frequency is away from interband transitions and therefore the quality factor and scattering intensity can be enhanced.

The ITO substrates were modified by the combination of nanosphere lithography and 120 keV Xe+ ion-bombardment to create nanopatterns with sharp boundaries between the irradiated and unirradiated (masked) regions. The nanopatterned surface has been analysed with SEM, AFM, and scanning tunnelling microscopy and spectroscopy (STM/STS). The refractive index of the unirradiated and irradiated ITO surfaces was determined by spectroscopic ellipsometry (SE). Our calculations for pattern formation has shown that the contour edges are as sharp as 20 nm, i.e., much shorter than the gold nanorod length (about 90 nm). The nanopattern appears in both the optical properties (refractive index as revealed by SE) and electrical properties (conductance as revealed by STM/STS) of the ITO layer. Therefore the utilized high-contrast surface patterning approach allows the modification of both the surface physical/chemical state and dielectric constant of ITO. These parameters determine the local environment of GNRs placed on the nanopatterned substrate.

Using correlative SEM and single particle dark-field optical scattering spectroscopy, the single particle scattering spectra of GNRs distributed over the nanopatterned ITO surface are investigated in detail. With this method one can resolve substrate inhomogeneity related damping and intensity variations in the spectra of individual GNRs at a length scale shorter than the GNRs themselves. The increased damping measured on fully irradiated areas of ITO can be explained by an excess of the chemical interface damping term due to irradiation-induced surface defect states. It was found that the surface nanopattern has profound influence on the homogeneous line width of the LSPR, depending on the asymmetric (rods overlapping the boundary between the implanted and masked zones) or symmetric (that is by bridging between two masked regions over an irradiated region) position of the GNR over the pattern. In the asymmetric case, even if only one of the two tips is located on irradiated area (corresponding to approximately 1/3 of the total nanorod length) the damping is found to be the same as for a GNR fully located on irradiated ITO. For the symmetric case, on the contrary, a more continuous increase of damping with the bridge, i.e., gap width can be inferred. Comparing the damping variations with the related intensity changes indicates that substrate inhomogeneity at such length scales results in a different behaviour of the LSPR than predicted by the classical damped harmonic oscillator model applied for nanoparticles encapsulated or homogeneously surrounded by molecular coatings.

An individual GNR in this case can be regarded as a plasmon ruler on the solid surface providing local information about its precise placement on the varying surface pattern with spatial sensitivity of few nanometres. The observed effect paves the way toward monitoring environmental changes on very short length scales.

The above results were summarized in a manuscript: „Gold Nanorod Plasmon Resonance Damping Effects on a Nanopatterned Substrate” and submitted to the Journal of Pysical Chemistry C, IF: 4.48 [24]. The reviewer report of this paper was positive recommending minor revision. Now the corrected manuscript is prepared and the paper is about re-submission. The submitted version of the manuscript is attached at the end of this report as Appendix.

Further works related to ion irradiation-induced changes and surface nanopatterning

Simulations with the TRIDYN code [L2] are underway to estimate the effect of ion beam-induced mixing and sputtering as driving force for atomic transport processes during ion irradiation of Au-silica core-shell NPs. In a related work we reported the validity of the ballistic ion beam mixing model in nanoscale atomic transport at Si/C interfaces as model structures using TRIDYN [25, 26].

In related works, we have shown the potential of the nanosphere lithography technique to prepare magnetic nanostructures with curved surface and special magnetic properties [27] and to introduce nanoscaled surface morphology and percolation barrier network into mesoporous silica coatings [28].

References (publications related to the project)

[1] S. Lugomer Z. Zolnai, A. L. Tóth, A. Deák, N. Nagy, Thin Solid Films 574, 136-145 (2015) IF: 1.76.

[2] M. Mayer, P. Malinsky, F. Schiettekatte, Z. Zolnai, NIM B 385, 65-73 (2016), IF: 1.39.

[3] Z. Zolnai, P. Petrik, A. K. Rossall, J. A. van den Berg, A. Deák, S. Pothorszky, G. Vértesy, L. Illés, and G. Battistig: The role of large-angle dual scattering in the MEIS analysis of gold nanostructures, The 23rd Int. Conf. on Ion Beam Analysis (IBA-2017), Shanghai, China, Oct 8-13, 2017, oral presentation

[4] Z. Zolnai, A. K. Rossall, J. A. van den Berg, A. Deák, S. Pothorszky, D. Zámbó, L. Illés, and G. Battistig: Large-angle dual scattering yield in the MEIS spectra of gold nanostructures, 9th Int. Workshop on High-Resolution Depth Profiling (HRDP9), Uppsala, Sweden, June 25-29, 2018, poster presentation

[5] Z. Zolnai, P. Petrik, A. Deák, S. Pothorszky, D. Zámbó, G. Vértesy, N. Nagy, A. K. Rossall and J. A. van den Berg: A three dimensional analysis of Au-silica core-shell nanoparticles using medium energy ion scattering 8th Int. Workshop on High-Resolution Depth Profiling (HRDP8), London, Ontario, Canada, Aug 7-11, 2016, poster presentation

[6] Z. Zolnai, G. Battistig, A. K. Rossall, J. A. van den Berg, A. Deák, S. Pothorszky, L. Illés, and G. Vértesy: Following ion irradiation-induced shape change of Au-silica core-shell nanospheres and nanorods by MEIS, The 23rd Int. Conf. on Ion Beam Analysis (IBA-2017), Shanghai, China, Oct 8-13, 2017, poster presentation

[7] A. K. Rossall, J. A. van den Berg, Z. Zolnai, P. Petrik, A. Deák, S. Pothorszky, G. Vértesy, L. Illés, and G. Battistig: Three-dimensional analysis of Au-silica core-shell nanoparticle clusters using medium energy ion scattering, The 23rd Int. Conf. on Ion Beam Analysis (IBA-2017), Shanghai, China, Oct 8-13, 2017, poster presentation

[8] J. Chandrappan M. Murray, T. Kakkar, P. Petrik, E. Agócs, Z. Zolnai, D. P. Steenson, A. Jha, G. Jose, Scientific Reports 5, 14037 (2015), IF: 5.23

[9] J. Chandrappan, M. Murray, P. Petrik, E. Agócs, Z. Zolnai, A. Tempez, S. Legendre, D. P. Steenson, A. Jha, G. Jose, Opt. Mater. Express 5, 2849 (2015), IF: 2.66

[10] Z. Zolnai, A. Deák, N. Nagy, D. Zámbó, S. Pothorszky, and A. Németh: A Three Dimensional Approach for Structural and Electrical Characterization of Planar Sets of Gold Nanoparticles, 7th Int. Conf. on Advanced Nanomaterials (ANM2016), Aveiro, Portugal, July 25-27, 2016

[11] Z. Zolnai, A. Deák, D. Zámbó, S. Pothorszky, N. Nagy, G. Battistig, and E. Kótai: Comprehensive Three Dimensional Ion Beam Analysis of Gold and Silica Nanoparticles Supported by Silicon Substrates, 22nd Int. Conf. on Ion Beam Analysis, Opatija, Croatia, June 14-19, 2015, poster presentation

[12] D. Zámbó, A. Deák, Periodica Polytechnica 60, 244-251 (2016), IF: 0.46

[13] S. Pothorszky, D. Zámbó, T. Deák, A. Deák, Nanoscale 8, 3523 (2016), IF: 7.36

[14] S. Pothorszky, D. Zámbó, D. Szekrényes, Z. Hajnal, A. Deák, Nanoscale 9, 10344 (2017), IF: 7.23

[15] D. Zámbó, G. Z. Radnóczi, A. Deák, Langmuir 31, 2662 (2015), IF: 3.99

[16] D. Zámbó, S. Pothorszky, D. F. Brougham, A. Deák, RSC Advances 6, 27151 (2016), IF: 3.29

[17] Ö. Sepsi, S. Pothorszky, T. M. Nguyen, D. Zámbó, F. Ujhelyi, S. Lenk, P. Koppa, A. Deák, Opt. Express 24, A424-A429 (2016), IF: 3.15

[18] N. Nagy, D. Zámbó, S. Pothorszky, E. Gergely-Fülöp, A. Deák, Langmuir 32, 963-971 (2016), IF: 3.99

[19] S. Pothorszky, D. Zámbó, A. Deák, Particle & Particle Systems Characterization 34, 1600291 (2017), IF: 4.38.
[20] D. P. Szekrényes, S. Pothorszky, D. Zámbó, Z. Osváth, A. Deák, J. Phys. Chem. C 122, 1706-1710 (2018), IF: 4.48.
[21] S. Pothorszky, D. Zámbó, Z. Hajnal and A. Deák: Patchy nanoparticle preparation and self-assembly, 31st Conference of the European Colloid and Interface Society, 3-8 September, 2017, Madrid, Spain, poster presentation
[22] D. P. Szekrényes, S. Pothorszky, D. Zámbó, Z: Hajnal, Z. Osváth, and A. Deák: Surface chemical patch formation and self-assembly investigated at the single particle level, 32nd Conference of the European Colloid and Interface Society (ECIS 2018), Ljubljana, Slovenia, 2-7 September, 2018, oral presentation
[23] D. P. Szekrényes, S. Pothorszky, D. Zámbó, Z. Hajnal, Z. Osváth, A. Deák: Patchy nanoparticles and their assemblies investigated at the single particle level, 11th Colloid Chemistry Conference, 28-30 May 2018, Eger, Hungary, oral presentation
[24] Z. Zolnai, D. Zámbó, Z. Osváth, N. Nagy, M. Fried, A. Németh, S. Pothorszky, A. Deák: Gold Nanorod Plasmon Resonance Damping Effects on a Nanopatterned Substrate, J. Phys. Chem. C, IF: 4.48, *submitted and reviewed, minor revision is recommended*
[25] G. Battistig, Z. Zolnai, A. Németh, P. Panjan, M. Menyhárd., J. Phys. D 49, 185303 (2016), IF: 2.77
[26] G. Battistig, S. Gurbán, G. Sáfrán, A. Sulyok, A. Németh, P. Panjan, Z. Zolnai, M. Menyhárd, Surf. Coat. Technol. 302, 320 (2016), IF: 2.14
[27] D. Merkel, D. Bessas, Z. Zolnai, R. Rüffer, A. I. Chumakov, H. Paddubrouskaya, C. Van Haesendonck, N. Nagy, A. L. Tóth, and A. Deák, Nanoscale 7, 12878-12887 (2015), IF: 7.76
[28] E. Albert, P. Basa, A. Deák, A. Németh, Z. Osváth, G. Sáfrán, Z. Zolnai, Z. Hórvölgyi, and N. Nagy, RSC Advances 5, 60041 (2015), IF: 3.29

Literature

[L1] Z. Hajnal, E. Szilágyi, F. Pászti, G. Battistig, Nucl. Instrum. Methods Phys. Res. B 118 (1996) 617.
[L2] Möller W and Posselt M 2001 TRIDYN_FZR User Manual FZR-317 (Dresden: Forschungzentrum Rossendorf)

<u>Appendix</u>

At the end of this report we attach the manuscript submitted to Journal of Pysical Chemistry C and returned with the reviewer's decision as accepted with minor revision.
Parameters of the manuscript:

Z. Zolnai, D. Zámbó, Z. Osváth, N. Nagy, M. Fried, A. Németh, S. Pothorszky, A. Deák:
Gold Nanorod Plasmon Resonance Damping Effects on a Nanopatterned Substrate

Appendix – manuscript for J. Phys. Chem. C before minor revision

Gold Nanorod Plasmon Resonance Damping Effects on a Nanopatterned Substrate

*Zsolt Zolnai[1], Dániel Zámbó[1], Zoltán Osváth[1], Norbert Nagy[1], Miklós Fried[1], Attila Németh[2], Szilárd Pothorszky[1], András Deák[1]**

[1]Institute of Technical Physics and Materials Science, HAS Centre for Energy Research, P.O. Box 49, H-1525 Budapest, Hungary

[2]Winger Research Centre for Physics, Institute for Particle and Nuclear Physics,

Konkoly-Thege M. str. 29-33, H-1121 Budapest, Hungary

KEYWORDS. Nanopatterning, gold nanorod, damping, scattering spectroscopy, substrate effect

ABSTRACT

Substrate properties might significantly influence the scattering spectra of supported plasmonic nanoparticles due to different damping mechanisms. In this work ITO substrates are modified by the combination of nanosphere lithography and ion-bombardment to create a nanopattern with sharp boundaries between the irradiated and masked regions. The single particle scattering spectra of gold nanorods distributed over the nanopattern are investigated in detail. For nanorods located purely on either the masked or implanted areas, the spectra can be adequately interpreted in terms of a classical damped harmonic oscillator model, taking the chemical interface damping into account. When the particles overlap the masked and irradiated areas, however, markedly different behavior is found depending on the actual arrangement. For the rods experiencing a symmetric inhomogeneity (that is by bridging between two masked regions), damping varies smoothly with the extent of substrate inhomogeneity. For the asymmetric case (rods overlapping the boundary between the implanted and masked zones) a sudden increase of the damping is found, which is rather independent on the specific extent of substrate inhomogeneity. Comparing the damping variations with the related intensity changes indicates that substrate inhomogeneity at such length scales results in a different behavior than predicted by the classical damped harmonic oscillator model applied for nanoparticles encapsulated or homogeneously surrounded by molecular coatings.

INTRODUCTION

When an electromagnetic wave is impinging on a metal nanoparticle, it can induce localized surface plasmon resonances (SPR) related to the collective coherent oscillations of conduction electrons. The spectral position of the SPR shows strong dependence on nanoparticle size, shape, gap between neighboring particles, composition, and dielectric environment.[1–4] This

variability offers a wide range of applications such as imaging, sensing, local heating, enhanced Raman scattering, or nanoscale manipulation of light.[5–7] In addition to the spectral position of the SPR, another key feature for applications is the SPR width, Γ, that is the damping parameter. When the SPR frequency is away from the interband transitions, as in silver nanospheres and in gold nanorods for the longitudinal SPR (LSPR), it is much narrower, a situation especially interesting for applications.[8,9] In this case the quality factor Q, that sets the enhancement of the optical response and of the local field in and around the particle, is enhanced. This is because $Q = \Omega_R/\Gamma$ (Ω_R is the plasmon resonance frequency), and Γ is decreased. Previous studies resulted in the following expression for the plasmon line width Γ in the absence of interband electron-hole pair excitations:[10,11]

$$\Gamma = \Gamma_b + \Gamma_{rad} + \Gamma_s \quad (1)$$

The first term is the bulk nonradiative damping which describes the scattering of electrons with thermal phonons, electrons, impurities, defects, etc., and converts the absorbed light into heat.[12–14] It is assumed that Γ_b in the GNRs is the same as in the bulk material, and Γ_b = 72 meV.[11,15] The second term describes radiation damping, i.e., plasmon decay by secondary light emission.[12,13] The third term is the combined surface scattering and chemical interface damping (CID) term, and can be calculated as:

$$\Gamma_s = \frac{Av_F}{L_{eff}} \quad (2)$$

Here v_F is the Fermi velocity, A is the combined surface scattering and CID parameter, and L_{eff} is the effective path length of electrons to the surface, respectively. Electron surface scattering takes into account scattering of electrons at the surface of the GNR while CID considers an additional damping by changing the chemical interface of the GNR.[16–18] As it was shown, CID depends on L_{eff} in the same way as electron-surface scattering.[19] Previously the proportionality constant A has been determined for different chemical environments that fully surround the GNRs and values of A = 0.3, A = 0.46, and A = 0.95 has been found for CTAB (cetyltrimethylammonium bromide), DDT (dodecanethiol) coated GNRs and SiO_2 encapsulated GNRs, respectively, considering an L_{eff} parameter of $L_{eff} = D\sqrt{AR}$, where D is the rod diameter.[10,11,15] Because of the different plasmon damping mechanisms, Γ depends on the nanoparticle shape, size, material, and the surrounding environment. The overall linewidth Γ measured in ensemble nanoparticle studies is broadened because of size and shape distributions of the Au particles in the ensemble. Consequently, single particle spectroscopy studies are especially well suited to relate the line widths to different plasmon damping processes.

The main advantage of using nanorods in single-particle scattering studies is that their LSPR is away from the interband transitions, hence the longitudinal plasmon resonance oscillation shows up as an almost-Lorentzian line in the energy domain. The scattering cross-section σ_{sca} and the LSPR peak can be described by three independent parameters: the central frequency Ω_R, the full width at half-maximum Γ, and the area Ξ, which can be obtained from Lorentzian fit in a straightforward manner:

$$\sigma_{sca}(\omega) = \Xi \frac{\Gamma/2\pi}{(\omega-\Omega_R)^2+(\Gamma/2)^2} \quad (3)$$

Plasmon-based devices and future optoelectronic integration require the attachment of metal nanocrystals onto various substrates, which generally breaks the symmetry of the dielectric

environment surrounding the nanoparticles.[20,21] Here the understanding of surface damping and chemical interface damping processes as well as quality factor change for the supported nanoparticles becomes especially important, for instance, fabrication of nanostructures made of noble metals using electron beam lithography requires an adhesion layer.[22] Due to chemical interface damping strong spectral broadening and reduced field enhancement can be observed in linear relation with the adhesion film thickness.[23]

An approach to nanoscale manipulation is to break the lateral homogeneity of the substrate, e.g., by its patterning with charged particle – ion or electron – beams. Such technique allows guided assembly of single nanoparticles during their deposition to the substrate. As it was shown, ion irradiation leads to change of the physical-chemical properties of the substrate and either positive or negative deposition of gold particles to assigned regions can be achieved due to the modified interface between the substrate and the nanoparticle.[24] Nevertheless, in that case SPR properties and surface modification-induced chemical interface damping effects on the plasmonic nanoparticles have not been studied.

In general, nanopatterning of a surface which supports plasmonic nanoparticles introduces twofold asymmetry to their environment. The effect of the substrate on SPR can be taken into account, e.g., by the mirror charge model based on polarization and charge accumulation in the dielectric substrate under the nanoparticle.[20] In the substrate plane, however, a periodic nanopattern introduces asymmetry as a rapid change of the local environment (substrate surface termination, dielectric constant) in vicinity of the nanoparticles. Depending on the contrast mechanism of the patterning technique, the characteristic length scale of local environment change may be even bellow the NP size, especially for elongated NPs.[24,25] To date less attention was paid to the effect of nanopatterning of a substrate on the LSPR of elongated metallic nanoparticles deposited on it, but the damping and quality factor for nanorods can be expected to change significantly as the position of the nanoparticle on the nanopatterned substrate is varied.

In this work, silica nanosphere lithography (NSL) combined with Xe^+ ion irradiation is used to create high-contrast patterns on ITO. When ion bombardment is performed through a nanomask of ordered colloidal silica nanospheres than the structural, physical, and chemical properties of the substrate can be modified on the nanoscale as we have shown earlier.[25–28] For the present ITO-gold nanorod system, irradiation-induced surface defect states may alter the chemical interface and the local dielectric properties, hence changes in the plasmon resonance properties of GNRs can be expected when the particles are located on unirradiated or irradiated ITO surfaces. In this work, gold nanorods (GNRs) were distributed on the patterned ITO surface. Two special cases are investigated in detail to account for the effect of local substrate inhomogeneities on the optical properties: when the particles connect two masked areas (’bridging’) or when the particles are overlapping the boundary between the masked and irradiated areas (’overlapping’). Due to the high contrast of the surface modification method, the effect of local environment change in these special cases can be studied on a shorter length scale than the GNR length. We show that for GNRs the damping parameter (Γ) is very sensitive to the nature of short-range local environment change, and its different behavior for the symmetric ‘bridging’ and the asymmetric ‘overlapping’ cases is revealed.

EXPERIMENTAL SECTION

Ion irradiation

The 100 nm ITO layer/20 nm buffer layer/1 mm glass samples of 20×20 mm area were exposed to 120 keV Xe^+ ion bombardment at fluences of 1×10^{16} cm^{-2} and 3×10^{16} cm^{-2}. One set of samples was irradiated through an LB masks of colloidal silica particles with D = 400 nm, while another set was implanted on its full area, i.e., without using the silica mask.

Irradiation was performed at room temperature in the Heavy Ion Cascade Implanter at the Institute for Particle and Nuclear Physics of the Wigner Research Centre for Physics in Budapest. In both series of irradiation, an ion beam with typically millimeter dimensions was x–y scanned across the full sample surface in order to achieve good homogeneity of irradiation within the exposed area. The current density for the scanning beam was kept low two avoid beam heating effects.

AFM analysis

After removal of the silica nanoparticulate mask, the obtained ion irradiation-induced surface morphology on ITO was analyzed with an AIST–NT SmartSPM 1010 AFM setup operated in tapping mode. The measured AFM data were processed using the Gwyddion software (see http://gwyddion.net).

STM/STS analysis

Scanning tunneling microscopy (STM) and tunneling spectroscopy (STS) measurements were performed using a DI Nanoscope E operating under ambient conditions with mechanically-cut Pt/Ir (90/10%) tips. The STS measurements were acquired at feedback parameters of -1 V and 5 nA.

FESEM analysis

Field Emission Scanning Electron Microscopy (FESEM) analysis of the silica nanomask, the nanopatterned ITO surfaces, and the Au nanorods deposited on it was carried out by a 5 keV energy electron beam perpendicular to the sample surface with a LEO 1540 XB microscope.

Dark-field optical scattering spectroscopy

Single particle spectra have been measured using an upright optical microscope (Olympus BX51) combined with an aberration corrected imaging spectrometer (IsoPlane SCT 320 equipped with a PIXIS 400BRX cooled CCD camera, Princeton Instruments). The sample was mounted on an XYZ piezo stage for precise sample positioning (Physik Instrumente, P 545.3R8S). Illumination and scattered light collection were performed in epi-illumination using a 100× dark-field objective (Olympus MPlanFLN, NA=0.9).

Template particle synthesis and LB film deposition

Silica nanoparticles with 400 nm in diameter were synthesized by a slightly modified seed-mediated synthesis protocol.[29] 60 mL ethanol absolute (99.97%, VWR International Ltd.) was mixed with 1.56 mL ultrapure water (MilliQ, 18.2 MΩ·cm) and 9.4 mL ammonium hydroxide solution (28-30%, Reagent grade, Sigma-Aldrich) in a laboratory glass bottle and stirred vigorously for 20 minutes. Seed silica nanoparticles (LUDOX AS-40, 40wt% in suspension, Sigma-Aldrich) were diluted 10.000-fold by ultrapure water and 256 μL was injected to the premixed solution and stirred continuously for 20 minutes. Afterwards, 1.8 mL silica precursor (tetraethyl orthosilicate, 98%, Sigma-Aldrich) was added to the solution and the reaction mixture was stirred gently for another 24 hours. The excess of ammonia was then removed by boiling and stirring the sol until the pH reached the value of 7. The particles were centrifuged (3000 rcf, 5 minutes) and redispersed in ethanol:chloroform mixture in 1:2 volume ratio. This solution was spread onto the water/air interface in a Wilhelmy film balance (KSV2000), compressed until 27 mN/m surface pressure and allowed to relax for 1 hour. The particles were deposited onto ITO-covered substrates (PGO GmbH., CEC020S) applying withdrawal speed of 7 mm/min and the films were dried and stored at room temperature. The diameter of the template particles was determined by DLS (441 ± 5 nm) and SEM (406 ± 4 nm).

Au nanorod synthesis and deposition

Cetyltrimethylammonium bromide (CTAB, 99%), sodium borohydride ($NaBH_4$, 99%), L-ascorbic acid (AA, >99%), silver nitrate ($AgNO_3$, >99%), sodium oleate (NaOL, ≥99%), hydrochloric acid (37%), and tetrachloroauric acid trihydrate (99.9%) were obtained from

Sigma-Aldrich. Gold nanorods with precisely tuned aspect ratio were synthesized by a binary surfactant mixture-assisted seeded growth protocol.[30] In the first step, a seed particle solution was prepared by mixing 1 mL 0.2 M CTAB and 1 mL 0.5 mM $HAuCl_4$ solution in a reaction vial. Under vigorous stirring, 0.2 mL $NaBH_4$ solution (containing 0.12 mL 0.01 M ice-cold $NaBH_4$ solution and 80 μL ultrapure water) was injected into the mixture, stirred for 2 minutes and left undisturbed for 30 minutes. The growth solution containing 0.9 g CTAB, 0.1543 g NaOL and 25 mL ultrapure water was heated to 50 °C and stirred until the components dissolved. Afterwards, the solution was cooled down to 30 °C and 1.8 mL 0.004 M $AgNO_3$ was injected and kept undisturbed for 15 minutes. Then 25 mL 1 mM $HAuCl_4$ solution was added and the system was stirred until 90 minutes at higher speed. 0.21 mL cc. HCl was added to the colorless solution and stirred at lower speed for 15 minutes. In the next step, 0.125 mL 0.064 M ascorbic acid solution was injected and shaken for several tens of seconds. Finally, 20 μL of seed-solution was added quickly, stirred for 30 seconds and kept undisturbed and stored at 28 °C water bath for 12 hours. The nanorods were purified by centrifuging (6000 rcf, 10 min) and redispersion in ultrapure water. After the removal of excess CTAB molecules, the particles were spin-casted onto the substrates from a diluted solution (5-fold) applying 1000 rpm for 30 seconds (Chemat Technology KW-4A) and dried under nitrogen flow.

RESULTS AND DISCUSSION

The 100 nm thick polycrystalline ITO layers supported by glass substrate were irradiated by 120 keV Xe^+ ions through a monolayer consisting of 400 nm diameter silica spheres to produce surface nanopatterns over a large area. The pattern of the nanomask is formed on the surface (see Figure S1) because Xe^+ ions can penetrate only in the holes formed between the masking silica nanospheres and cannot reach the ITO surface underneath the masked areas, as we have shown earlier.[25,27] As full-cascade Monte-Carlo simulation of the ion irradiation process for the given system shows, point defects are formed at the surface and in the deeper regions of ITO, due to displacement cascades initiated by the heavy Xe^+ ions (Figure S2). Therefore, atomic rearrangement and surface defects on the implanted areas of the ITO surface are expected to play a role when get into contact with GNRs. To check the effect of ion irradiation of ITO on the plasmon resonance properties of GNRs, two reference samples have been prepared and investigated: optical scattering spectra were measured on single nanorods located on a native ITO substrate and on implanted ITO samples, in the latter case maskless irradiation of the whole surface has been performed with 120 keV Xe^+ ions to a fluence of $3\times10^{15}/cm^2$.

Figure S4 shows the distribution of the aspect ratios (AR) determined from FESEM analysis for a representative set of GNRs. The average size of the nanorods is 91 nm × 36 nm. Figure 1 shows Γ values as a function of LSPR resonance wavelengths for individual GNRs on the native and implanted ITO surface. These parameters were determined from Lorentz fits of the measured spectra. The obtained differences in the LSPR peak positions are primarily due to the slightly different AR values of the GNRs. No significant dependence of Γ on the LSPR wavelength is found for both cases, which, is in agreement with previous studies obtained for Au nanorods (AR >2) on glass substrate, due to the plasmon resonance energy is away from the interband transition and Γ is not affected by interband electron-hole pair excitations.[9] Nevertheless, Γ is significantly higher for the implanted ITO sample by 33 meV in average, as Γ = 99±5 meV for the native and Γ = 132±4.5 meV for the implanted reference sample. This readily indicates that plasmon damping at the longitudinal resonance increases as a result of substrate implantation. Since bulk damping, radiation damping, and electron surface-scattering contributions to Γ can be assumed to be the same, it can be inferred that irradiation-induced surface defect states generated by the energetic Xe^+ ions make a

difference to the chemical interface of the ITO-GNR system, leading to an increased proportionality constant A in Eq. 2. Since L_{eff} is not affected by the surrounding of the NRs, the change of the combined surface scattering and CID term, ΔA, can be expressed as:

$$\Delta\Gamma = \frac{\Delta A v_F}{L_{eff}} \quad (4)$$

With $\Delta\Gamma$ = 33 meV this results in ΔA = 0.29 upon ion irradiation-induced modification of ITO. This is comparable with the values obtained for CTAB and DDT coated GNRs,[10,15] and is relatively high when considering that the molecular coatings cover the full surface of the GNR, while in the present case the contact between the modified ITO surface and the Au particle is much more limited.

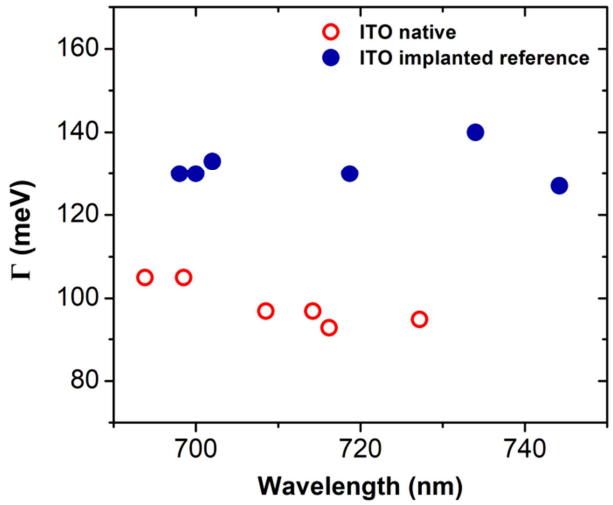

Figure 1. Γ values as a function of resonance wavelength determined from Lorentz fits of single-particle dark-field optical scattering spectra of Au nanorods deposited on native (unirradiated) ITO surface and on a maskless ITO surface implanted on its full area with 120 keV Xe^+ ions to a fluence of $3\times10^{15}/cm^2$.

After analysis of the reference and full-area irradiated ITO samples, the nanopatterned ITO surface and the optical properties of Au nanoparticles deposited on it have been analyzed. Figure 2 shows AFM images of the native, and the ion beam-nanopatterned ITO surface. In panel (a) the polycrystalline structure of the native ITO layer can be observed. After the ion irradiation process the pattern of the silica nanomask can be clearly seen in Figure 2b. Here the circular areas represent the unirradiated (masked) regions while the surrounding regions are the irradiated zones. The height difference between the two areas can be attributed to the ion beam-induced sputtering effect. As full-cascade SRIM (www.srim.org) simulations show, for 120 keV Xe^+ irradiation into ITO 17 atoms/ion are sputtered out from the target when displacement cascades reach the surface atoms (Figure S2). This results in about 6 nm ITO sputtered out from the irradiated areas and this value is in good agreement with the AFM pattern.

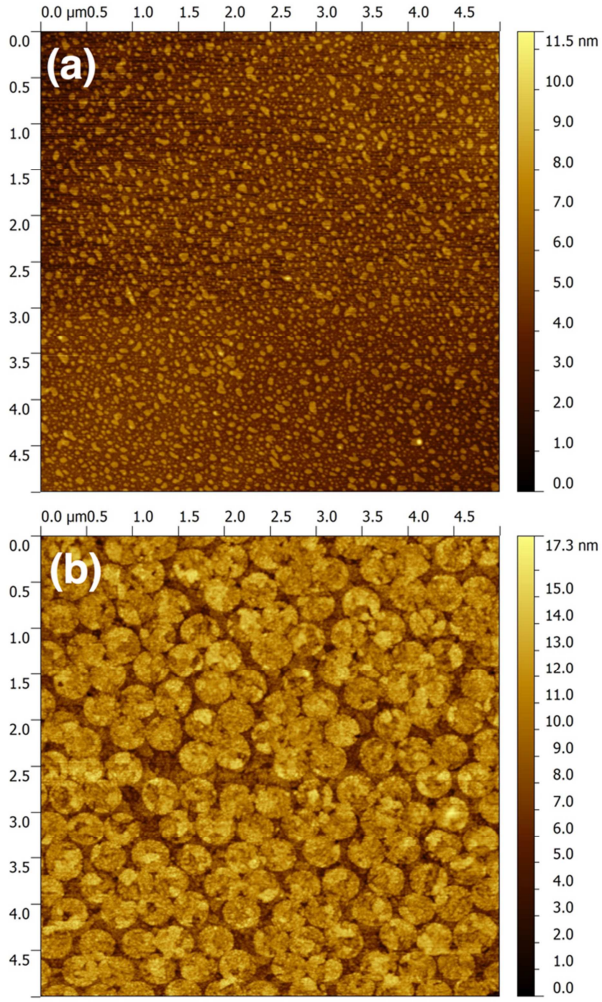

Figure 2. Atomic Force Microscopy (AFM) image of (a) unirradiated (native) and (b) ion beam-irradiated ITO surface. Ion bombardment has been performed with 120 keV Xe^+ ions to a fluence of $3\times10^{15}/cm^2$ through a nanomask of ordered silica particles with diameter of 400 nm. For the unirradiated surface the polycrystalline structure of the ITO layer can be observed. After the ion irradiation process the pattern of the silica nanomask can be clearly seen on the surface. Higher circular areas represent the unirradiated (masked) regions while the surrounding lower regions are the irradiated zones.

ITO is a wide band gap material with E_g = 3.5-4 eV that exhibits the special property of a high optical transmittance in the visible region of the spectrum combined with a high electrical conductivity. [31,32] As it was previously shown, ion irradiation leads to degradation of the optical transparency and electrical conductivity of polycrystalline ITO layers.[31–34] Ion irradiation-induced changes in the optical properties as the refractive index, *n*, and extinction coefficient, *k*, have been followed by spectroscopic ellipsometry (SE) measurements. As Figure S5 shows, the refractive index at around the plasmon resonance wavelength of GNRs (ca. 790 nm) increased from n = 1.55 to n = 1.8, and n = 1.85 for fluences of 1×10^{16} cm^{-2} and 3×10^{16} cm^{-2} after the ion irradiation process. The extinction coefficient increased about one order of magnitude, however, still giving a small value of k = 0.1. The n and k lateral patterns are expected to follow the nanomask pattern on ITO with transition zones of about 20 nm width, considering ion beam proximity effects at the masking silica particle edges, see the schematics in the Supporting Information (Figure S3). Therefore, the n and k values in the vicinity of GNRs can vary on a much shorter scale than the GNR length. We estimate similar

changes in lateral direction for the amount of irradiation-induced defects at the ITO surface, considering the SRIM trajectory patterns traced out by the bombarding ions and recoiled target atoms in the collision cascades.

The effect of ion irradiation on the electrical properties of ITO was characterized by Scanning tunneling microscopy (STM) and tunneling spectroscopy (STS) measurements. Figure 3a shows STM image of the nanopatterned ITO surface and Figure 3b depicts tunneling conductance plots probed by STS measurements on the unirradiated and irradiated regions of ITO. In the STM image the boundaries between unirradiated and irradiated areas can be clearly seen. The morphology and the height changes agree well with the AFM results. The polycrystalline structure is observed with even higher resolution. The red and black dots represent the positions where the current (I)-voltage (V) curves were recorded. The I-V characteristics shown in Figure 3b are averages of 25 consecutive spectra taken at the same position on the sample. A band gap of 3.5 eV is observed, with the conduction band minimum around 0.5 eV. It is clear from the spectra in Figure 3b that the tunneling conductance of the native ITO regions (red curve) is larger than the one of the bombarded regions (black curve) at all energies. This is in agreement with the fact that ion irradiation introduces defects which decrease the conductance of the irradiated regions and changes the physical/chemical properties of the ITO surface due to atomic rearrangement and the formation of surface defects. It has to be emphasized, that the ion-irradiation induced pattern has an excellent contrast at the interface.

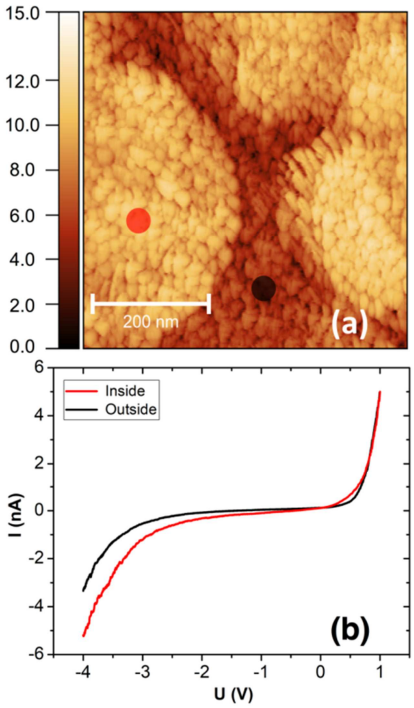

Figure 3 (a) Scanning tunneling microscopy (STM) image of the nanopatterned ITO surface and (b) tunneling conductance plots probed by scanning tunneling spectroscopy (STS) measurements on the unirradiated (inside) and irradiated (outside) regions of ITO. In (a) red and black dots represent the positions where I-V curves were measured. The color bar in (a) shows the values in the dimension of nm.

Targeted search for two main rod/pattern orientational configurations has been performed in the FESEM to identify particles of interest (also see Scheme 1): *(i) Bridging*: the two tips of the Au rod are located on two adjacent unirradiated areas separated by an irradiated area

(narrow gap) under the rod center. The bridging configuration is considered to be symmetric, i.e., the gap center coincides with the nanorod center. *(ii) Overlapping*: one tip of the Au rod is located on unirradiated while the other tip is on neighboring irradiated area. Additionally, particles positioned entirely on masked or irradiated areas have been identified, to serve as an internal reference and are denominated as 'inside' and 'outside' arrangements, respectively.

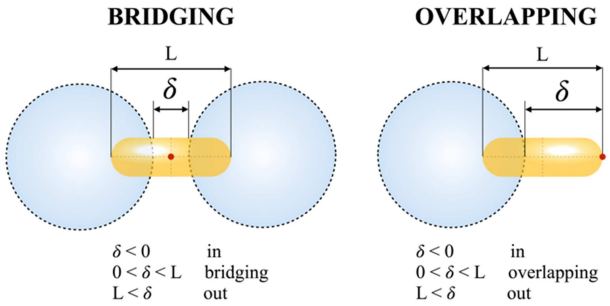

Scheme 1. Schematics of the ITO nanopattern-gold nanorod (GNR) arrangement geometry for symmetric bridging and asymmetric overlapping configurations. The distance δ is measured between the reference point of the GNR (red dot) and the perimeter of the circular unirradiated area (dotted line). Negative δ values mean that the GNR is inside the circular (masked) area.

Correlative FESEM and single particle optical scattering measurements allow to relate the position of individual GNRs on the nanopatterned surface with their optical scattering spectra in a quantitative way. Figure 4 shows the single particle scattering spectra of selected nanorods that represent the above discussed cases for demonstration, together with the Lorentzian fits. The FESEM micrographs show the spatial arrangement of the nanorods over the implanted/non-implanted regions of the nanostructured substrate. The intensities are normalized to the LSPR peaks for better comparability. For the nanopatterned ITO-GNR system damping is increased on the irradiated, 'outside' area (average Γ = 138 meV) compared to the unirradiated 'inside' area (average Γ = 108 meV), which is consistent with the results obtained on the maskless implanted ITO and native reference surface. The slight deviation of these values compared to the reference values (Figure 1) maybe due to the different history of the samples, since the experimental realization of the nanopatterns involved several additional technological steps. The resulting $\Delta\Gamma$ = 30 meV translates to ΔA = 0.26 for the combined surface scattering and CID parameter.

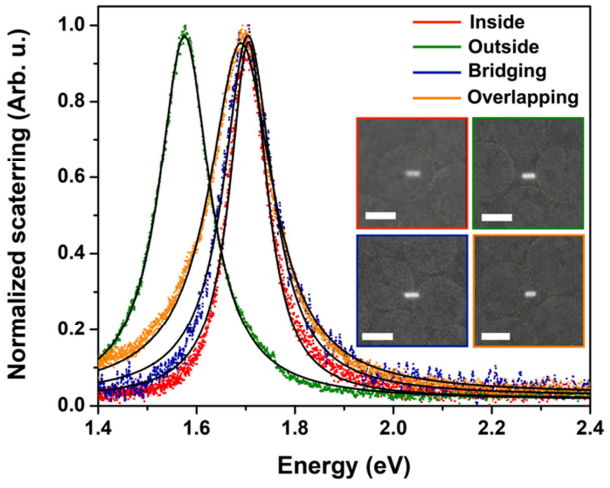

Figure 4. Normalized single-particle dark-field optical scattering spectra of Au nanorods located at different positions on an ion beam-nanopatterned ITO surface. Solid lines show Lorentzian fits. Inset: FESEM micrographs of the Au nanorods corresponding to the optical scattering spectra; the circular dashed lines show boundaries between irradiated and unirradiated areas, the scale bars represent 200 nm.

In the following we show how the optical scattering properties vary as a function of the relative position of the nanorod with respect to the nanopattern for both the bridging and overlapping cases. The spatial arrangements of the individual nanoparticles have been quantified based on the schematics shown in Scheme 1. This approach allows to quantitatively account for the symmetric bridging and asymmetric overlapping configurations based on the distance between the center or the tip of the GNR (red dot) and the border between the implanted/masked regions (dashed circle). Besides damping, the intensity of the resonance related to the quality factor $Q = \Omega_R/\Gamma$ (plasmon resonance energy divided by the damping) can be also obtained, since the intensity scales with Q^2 for a damped harmonic oscillator.[10]

Figure 5 shows the change of Γ and Q^2 (related to single particle optical scattering intensity) as a function of the gap width for symmetric bridging configuration. Clearly, changes in Γ can be resolved as the substrate inhomogeneity varies at a spatial extent smaller that the nanorod length itself. Upon increasing the gap from zero to the rod length, the gradual increase of Γ from about 112 meV to 146 meV can be observed over the approximate range of 0-100 nm gap size. On the other hand, Q^2 drops abruptly already for a 25 nm gap. This abrupt drop suggests the sudden change of the environment determining the strength of the plasmon resonance oscillation as the gap opens. This environmental change might have two main contributions. First, the variation in the physical/chemical state of the underlying ITO interface that occurs along the long axis of the particle since the particle bridges unirradiated-irradiated-unirradiated areas (Figure 3 inset). Second, the dielectric function of the ITO layer (down to ca. 70 nm in depth) increases upon ion-irradiation (Figure S5), hence a refractive index change along the particle long axis can be anticipated. Proximity effects during ion irradiation for a 20 nm gap can reduce the effective fluence by 20% (Figure S3) in the gap region, but SE measurements indicate that even when the fluence is decreased by the factor of 3, there is no significant change in the dielectric function of irradiated ITO. Hence, the extent of refractive index change in the gap-region due to irradiation can be regarded as identical for all gap sizes. Consequently, the effective refractive index at the substrate side along the nanorod increases with the gap width.

In agreement with earlier results, the increased damping is accompanied by the drop of the plasmon resonance intensity (i.e., Q^2) and it was also shown that the increase of the refractive index of the surrounding medium increases the scattering intensity for Au nanorods.[10] A scattering intensity increase of about 4% was reported when a single nanorod (27×81 nm) was covered with a monolayer of DDT molecules, causing an increase of about 8% in the refractive index. In the present work almost 20% increase of the refractive index of ITO was found by SE after ion irradiation. It can be anticipated that in the present case the interplay between the Au/ITO interface damping induced decrease and the refractive index induced increase gives the overall intensity change. For small gaps the domination of the damping contribution can be inferred, while for wider gaps the refractive index change seems to compensate the effect of increased damping.

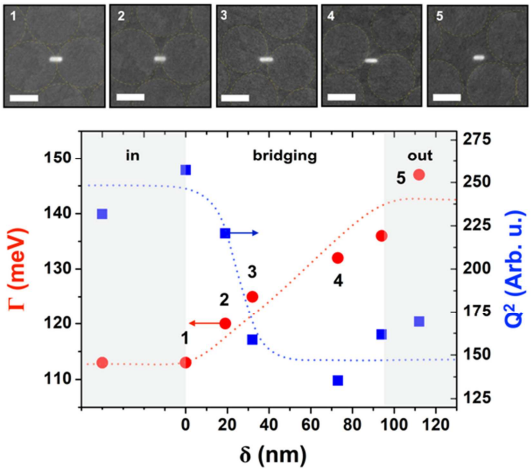

Figure 5. Top: FESEM micrographs of the Au nanorods bridging two non-implanted areas over an implanted one, corresponding to the data points labelled 1-5; scale bars represent 200 nm. Bottom: Γ and Q^2 (scattering intensity) values as a function of the gap width, that is, the width of the irradiated area under the rods. Dashed lines are guidelines.

For GNRs in overlapping configuration a somewhat different behavior of Γ and Q^2 vs. the particle position can be observed (Figure 6). Here the more abrupt increase of Γ is followed by a gradual decrease of Q^2 as the rod leaves the masked area of the ITO substrate. As one of the tips of the rod leaves the unirradiated to the irradiated zone by about 30 nm (ca. one third of the rod length), Γ abruptly increases from about 112 meV to 146 meV and does not change significantly for further movement of the GNR. The abrupt change of Γ compared to the bridging-arrangement supports that the location (local environment) of the nanorod tip has a profound influence on damping, since at the wavelength of the longitudinal plasmon resonance the high-intensity near field region is concentrated at the tips of the nanorod. It has to be emphasized, that already if one of the nanorod tips is located on irradiated ITO, Γ shows the value characteristic for the outside configuration. In contrast to the bridging case, for overlapping particles Q^2 changes gradually as a function of δ connecting smoothly the 'inside' and 'outside' configuration points with Q^2 values of about 230 and 130, respectively. This means the drop of the quality factor from 15.3 to 11.5. The decrease of Q^2 can already be observed before the jump in the damping Γ occurs.

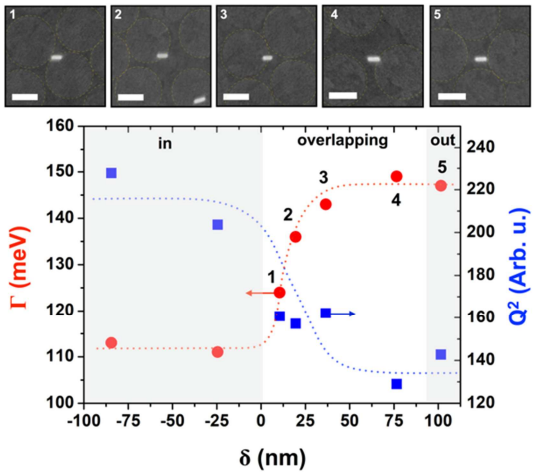

Figure 6. Top: FESEM micrographs of Au nanorods in overlapping configuration, corresponding to the data points labelled 1-5; scale bars represent 200 nm. Bottom: Γ and scattering intensity values vs. the distance of nanorod tip from the perimeter of the circular

unirradiated areas for Au nanorods located in asymmetric overlapping configuration on the nanopatterned ITO surface. Dashed lines are guidelines.

In summary, the change of Γ and Q^2 (scattering intensity) are not completely simultaneous when the nanorod position is varied over the nanopattern on a length scale smaller than the nanorod length. For both the bridging and overlapping case, the change of Q^2 seems to outrun the Γ change. On the other hand, an abrupt change of the intensity is accompanied by the gradual change of Γ and vice versa, for the bridging and overlapping configurations. Γ is very sensitive on the nature of the surface underneath the nanorod tip: it changes abruptly for the overlapping case (despite only one of the tips is located on an implanted area), while a smoother transition is observed as a function of the gap for the bridging-configuration, where both tips are located on unirradiated areas.

Usually, if the change of the surrounding environment is homogeneous over the nanorod length, e.g., when nanorods are encapsulated or fully covered by molecular coatings, as well as in slowly varying environments, abrupt changes in the parameters determining the plasmon resonance and optical scattering properties within the nanorod dimensions do not occur.[10,11,15] In the present case the 'inside' and 'outside' configuration represent homogeneous environment under the nanorods. However, for GNRs in bridging and overlapping arrangement the underlying substrate changes along the nanorod long axis, thus giving a longitudinal inhomogeneity of the environment with sharp boundaries. Considering the dielectric and surface properties of the substrate, the main difference between the two arrangements is related to symmetry: the bridging configuration is symmetric with two transition zones, while the overlapping configuration is asymmetric with only one transition zone upon crossing the unirradiated-irradiated zone border. Such markedly different conditions may impact the oscillation properties of the conduction electrons along the GNR long axis. For instance, asymmetric mirror charge-induced coupling to the substrate can be considered for the overlapping configuration, due to the different dielectric and conductance properties of the irradiated and unirradiated sections of ITO.[20] As Figures 5 and 6 show, abrupt changes in Γ and the intensity occur at the transition zone and here the two quantities are not so strongly correlated as it is predicted by the damped harmonic oscillator model which describes LSPR for GNRs with homogeneous surrounding environment. Detailed optical simulation of the electric field and charge density distribution accounting for the substrate inhomogeneities is however needed to unambiguously identify the origin of the observed dependence of the damping parameter and spectral intensity obtained for the different geometrical arrangements on the nanostructured substrate.

CONCLUSION

The utilized high-contrast surface patterning approach allows the modification of both the surface physical/chemical state and refractive index of ITO. With this method one can resolve substrate inhomogeneity related damping and intensity variations in the spectra of individual gold nanorods at a length scale shorter than the nanorods themselves. The increased damping measured on irradiated areas can be explained by an excess of the chemical interface damping term due to irradiation-induced surface defect states. It was found that the surface nanopattern has profound influence on the homogeneous line width of the LSPR, depending on the asymmetric or symmetric position of the GNR over the pattern. In the asymmetric case, even if only one of the two tips is located on irradiated area (corresponding to approximately 1/3 of the total nanorod length) the damping is found to be the same as for a GNR fully located on irradiated ITO. For the symmetric case, on the contrary, a more continuous increase of damping with the extend of inhomogeneity can be inferred. With the appearance of substrate

inhomogeneity, the intensity variation follows the expected trend, but its change is not completely simultaneous with the change of damping. This behavior is different than found for GNRs homogeneously surrounded by molecular coatings, where the intensity and line width change in a strongly coupled manner as predicted by the classical damped harmonic oscillator model.

ASSOCIATED CONTENT

Supporting Information. Details on the nanopatterning of ITO layers by masked ion irradiation; FESEM micrograph of the Langmuir-Blodgett monolayer of colloidal silica particles deposited on ITO and on the nanopatterned ITO surface; distribution of the aspect ratios of Au nanorods as evaluated from FESEM analysis; results of spectroscopic ellipsometry (SE) analysis; results of full-cascade SRIM simulations: the depth distribution of 120 keV Xe^+ ions and vacancy depth distribution; proximity effect calculations for the bridging configuration (PDF).

AUTHOR INFORMATION

Corresponding Author

* andras.deak@energia.mta.hu; +36 1 392 2602

Author Contributions

The manuscript was written through contributions of all authors. All authors have given approval to the final version of the manuscript.

ACKNOWLEDGMENT

The project was supported by the Hungarian Scientific Research Fund K-112114 and K-119532, M-ERA.NET-WaterSafe (Nr. 39/2016) and received funding from the Hungarian Academy of Sciences (INFRA 2016).

REFERENCES

(1) Oldenburg, S.; Averitt, R.; Westcott, S.; Halas, N. Nanoengineering of Optical Resonances. *Chem. Phys. Lett.* **1998**, *288* (2–4), 243–247.

(2) Kelly, K. L.; Coronado, E.; Zhao, L. L.; Schatz, G. C. The Optical Properties of Metal Nanoparticles: The Influence of Size, Shape, and Dielectric Environment. *J. Phys. Chem. B* **2003**, *107* (3), 668–677.

(3) Liz-Marzán, L. M. Tailoring Surface Plasmons through the Morphology and Assembly of Metal Nanoparticles. *Langmuir* **2006**, *22* (1), 32–41.

(4) Wang, F.; Shen, Y. R. General Properties of Local Plasmons in Metal Nanostructures. *Phys. Rev. Lett.* **2006**, *97* (20).

(5) O'Neal, D. P.; Hirsch, L. R.; Halas, N. J.; Payne, J. D.; West, J. L. Photo-Thermal Tumor Ablation in Mice Using near Infrared-Absorbing Nanoparticles. *Cancer Lett.* **2004**, *209* (2), 171–176.

(6) Aćimović, S. S.; Kreuzer, M. P.; González, M. U.; Quidant, R. Plasmon Near-Field Coupling in Metal Dimers as a Step toward Single-Molecule Sensing. *ACS Nano* **2009**, *3* (5), 1231–1237.

(7) Hatab, N. A.; Hsueh, C.-H.; Gaddis, A. L.; Retterer, S. T.; Li, J.-H.; Eres, G.; Zhang, Z.; Gu, B. Free-Standing Optical Gold Bowtie Nanoantenna with Variable Gap Size for Enhanced Raman Spectroscopy. *Nano Lett.* **2010**, *10* (12), 4952–4955.

(8) Klar, T.; Perner, M.; Grosse, S.; von Plessen, G.; Spirkl, W.; Feldmann, J. Surface-Plasmon Resonances in Single Metallic Nanoparticles. *Phys. Rev. Lett.* **1998**, *80* (19), 4249–4252.

(9) Sönnichsen, C.; Franzl, T.; Wilk, T.; von Plessen, G.; Feldmann, J.; Wilson, O.; Mulvaney, P. Drastic Reduction of Plasmon Damping in Gold Nanorods. *Phys. Rev. Lett.* **2002**, *88* (7).

(10) Foerster, B.; Joplin, A.; Kaefer, K.; Celiksoy, S.; Link, S.; Sönnichsen, C. Chemical Interface Damping Depends on Electrons Reaching the Surface. *ACS Nano* **2017**, *11* (3), 2886–2893.

(11) Juvé, V.; Cardinal, M. F.; Lombardi, A.; Crut, A.; Maioli, P.; Pérez-Juste, J.; Liz-Marzán, L. M.; Del Fatti, N.; Vallée, F. Size-Dependent Surface Plasmon Resonance Broadening in Nonspherical Nanoparticles: Single Gold Nanorods. *Nano Lett.* **2013**, *13* (5), 2234–2240.

(12) Wokaun, A.; Gordon, J. P.; Liao, P. F. Radiation Damping in Surface-Enhanced Raman Scattering. *Phys. Rev. Lett.* **1982**, *48* (14), 957–960.

(13) Grigorchuk, N. I. Radiative Damping of Surface Plasmon Resonance in Spheroidal Metallic Nanoparticle Embedded in a Dielectric Medium. *J. Opt. Soc. Am. B* **2012**, *29* (12), 3404.

(14) Kolwas, K.; Derkachova, A. Damping Rates of Surface Plasmons for Particles of Size from Nano- to Micrometers; Reduction of the Nonradiative Decay. *J. Quant. Spectrosc. Radiat. Transf.* **2013**, *114*, 45–55.

(15) Novo, C.; Gomez, D.; Perez-Juste, J.; Zhang, Z.; Petrova, H.; Reismann, M.; Mulvaney, P.; Hartland, G. V. Contributions from Radiation Damping and Surface Scattering to the Linewidth of the Longitudinal Plasmon Band of Gold Nanorods: A Single Particle Study. *Phys. Chem. Chem. Phys.* **2006**, *8* (30), 3540.

(16) Kreibig, U.; Vollmer, M. *Optical Properties of Metal Clusters*; Springer series in materials science; Springer: Berlin; New York, 1995.

(17) Voisin, C.; Del Fatti, N.; Christofilos, D.; Vallée, F. Ultrafast Electron Dynamics and Optical Nonlinearities in Metal Nanoparticles. *J. Phys. Chem. B* **2001**, *105* (12), 2264–2280.

(18) Zijlstra, P.; Paulo, P. M. R.; Yu, K.; Xu, Q.-H.; Orrit, M. Chemical Interface Damping in Single Gold Nanorods and Its Near Elimination by Tip-Specific Functionalization. *Angew. Chem. Int. Ed.* **2012**, *51* (33), 8352–8355.

(19) Persson, B. N. J. Polarizability of Small Spherical Metal Particles: Influence of the Matrix Environment. *Surf. Sci.* **1993**, *281* (1–2), 153–162.

(20) Vernon, K. C.; Funston, A. M.; Novo, C.; Gómez, D. E.; Mulvaney, P.; Davis, T. J. Influence of Particle−Substrate Interaction on Localized Plasmon Resonances. *Nano Lett.* **2010**, *10* (6), 2080–2086.

(21) Chen, H.; Ming, T.; Zhang, S.; Jin, Z.; Yang, B.; Wang, J. Effect of the Dielectric Properties of Substrates on the Scattering Patterns of Gold Nanorods. *ACS Nano* **2011**, *5* (6), 4865–4877.

(22) Debu, D. T.; Ghosh, P. K.; French, D.; Herzog, J. B. Surface Plasmon Damping Effects Due to Ti Adhesion Layer in Individual Gold Nanodisks. *Opt. Mater. Express* **2017**, *7* (1), 73.

(23) Jeppesen, C.; Mortensen, N. A.; Kristensen, A. The Effect of Ti and ITO Adhesion Layers on Gold Split-Ring Resonators. *Appl. Phys. Lett.* **2010**, *97* (26), 263103.

(24) Kolíbal, M.; Konečný, M.; Ligmajer, F.; Škoda, D.; Vystavěl, T.; Zlámal, J.; Varga, P.; Šikola, T. Guided Assembly of Gold Colloidal Nanoparticles on Silicon Substrates Prepatterned by Charged Particle Beams. *ACS Nano* **2012**, *6* (11), 10098–10106.

(25) Nagy, N.; Zolnai, Z.; Fülöp, E.; Deák, A.; Bársony, I. Tunable Ion-Swelling for Nanopatterning of Macroscopic Surfaces: The Role of Proximity Effects. *Appl. Surf. Sci.* **2012**, *259*, 331–337.

(26) Nagy, N.; Pap, A. E.; Horváth, E.; Volk, J.; Bársony, I.; Deák, A.; Hórvölgyi, Z. Large Area Self-Assembled Masking for Photonic Applications. *Appl. Phys. Lett.* **2006**, *89* (6), 063104.

(27) Zolnai, Z.; Nagy, N.; Deák, A.; Battistig, G.; Kótai, E. Three-Dimensional View of the Shape, Size, and Atomic Composition of Ordered Nanostructures by Rutherford Backscattering Spectrometry. *Phys. Rev. B* **2011**, *83* (23).

(28) Merkel, D. G.; Bottyán, L.; Tanczikó, F.; Zolnai, Z.; Nagy, N.; Vértesy, G.; Waizinger, J.; Bommer, L. Magnetic Patterning Perpendicular Anisotropy FePd Alloy Films by Masked Ion Irradiation. *J. Appl. Phys.* **2011**, *109* (12), 124302.

(29) Chen, S.-L.; Yuan, G.; Hu, C.-T. Preparation and Size Determination of Monodisperse Silica Microspheres for Particle Size Certified Reference Materials. *Powder Technol.* **2011**, *207* (1–3), 232–237.

(30) Ye, X.; Zheng, C.; Chen, J.; Gao, Y.; Murray, C. B. Using Binary Surfactant Mixtures To Simultaneously Improve the Dimensional Tunability and Monodispersity in the Seeded Growth of Gold Nanorods. *Nano Lett.* **2013**, *13* (2), 765–771.

(31) Vink, T. J.; Overwijk, M. H. F.; Walrave, W. The Active Dopant Concentration in Ion Implanted Indium Tin Oxide Thin Films. *J. Appl. Phys.* **1996**, *80* (7), 3734–3738.

(32) Haynes, T. E.; Shigesato, Y.; Yasui, I.; Taga, N.; Odaka, H. Ion Beam Modification of Transparent Conducting Indium-Tin-Oxide Thin Films. *Nucl. Instrum. Methods Phys. Res. Sect. B Beam Interact. Mater. At.* **1997**, *121* (1–4), 221–225.

(33) Morgan, D. V.; Salehi, A.; Aliyu, Y. H.; Bunce, R. W.; Diskett, D. Radiation Damage in Indium Tin Oxide (ITO) Layers. *Thin Solid Films* **1995**, *258* (1–2), 283–285.

(34) Shigesato, Y.; Paine, D. C.; Haynes, T. E. Lattice Defects in O^+ Implanted Tin-Doped Indium Oxide Films. *Jpn. J. Appl. Phys.* **1993**, *32* (Part 2, No. 9B), L1352–L1355.

TABLE OF CONTENTS GRAPHIC